ACS OMEGA

http://pubs.acs.org/journal/acsodf

Article

Discrimination of Six Flotation Kinetic Models Used in the Conventional Flotation and Carrier Flotation of −74 μm Coal Fines

Xiangning Bu,* Xuexia Wang, Shaoqi Zhou, Biao Li,* Hanhui Zhan, and Guangyuan Xie

Cite This: *ACS Omega* 2020, 5, 13813−13821

Read Online

ACCESS | Metrics & More | Article Recommendations | Supporting Information

ABSTRACT: In this study, experimental results of conventional flotation and carrier flotation were characterized by six commonly used flotation kinetic models. Two statistical criteria (coefficient of determination, R^2, and root mean square error, RMSE) were used for comparison of fitting performance of different models. All kinetic models tested gave good levels of goodness of fit, but the second-order model with rectangular distribution (model 6) provided the best fitting performance for the experimental data of conventional flotation and carrier flotation. On this basis, two parameters, that is, modified flotation rate constant (K_m) and selectivity index (SI), were used to evaluate the difference in flotation separation selectivity between conventional flotation and carrier flotation. Comparisons of K_m and SI values indicated that carrier flotation significantly improved the flotation rate constant of combustible materials and flotation separation selectivity of ultrafine coal (−74 μm). In addition, measurements of average bubble size and water recovery indicated that both the coalescence of bubbles and the drainage of liquid in the froth were promoted when coarse coal particles (contact angle >90°) were employed as the carrier to assist the flotation recovery of ultrafine particles, which in turn favored the inhibition effect of the entrainment of gangue materials in carrier flotation compared to conventional flotation.

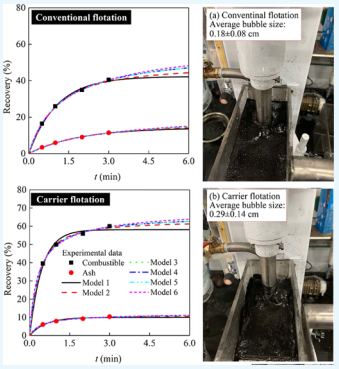

INTRODUCTION

Flotation is one of the most efficient methods for the beneficiation of fine ores and coal.[1] However, there is considerable evidence that both flotation recovery and rate constant decline steadily as particles fall below a critical size.[2] In general, the highest flotation rate constant and recovery of coal are seen on particles of an intermediate size range, for example, 250−74 μm;[3,4] although the flotation kinetics of ultrafine coal particles (−74 μm) is very low, this is attributed to the low collision probability between ultrafine particles and air bubbles resulting from the lack of inertia and the small kinetic energy of ultrafines.[5] According to various particle−bubble collision models, the flotation recovery of fine/ultrafine particles increases with increasing particle size.[2] Therefore, a large range of modified flotation processes, in which flotation was performed after increasing the apparent particle size of target fine/ultrafine particles, were developed. These processes are selective flocculation, agglomerate flotation, electrocoagulation/flotation, precipitate flotation, oil flotation, shear-flocculation/flotation, and carrier flotation,[1,6] among which carrier flotation distinguishes itself from other processes as it has an advantage in reducing the unselective entrainment of gangue particles into the concentrate.[7]

Carrier flotation can be considered as a hydrophobic flocculation−flotation process in which fine hydrophobic particles are first preferentially collected by larger hydrophobic carrier particles so that the apparent separation size of valuable particles increases to the extent that allows them to be efficiently recovered by conventional flotation. Chia and Somasundaran examined the stability of aggregates consisting of anatase and calcite particles formed under various flotation chemistry and hydrodynamic conditions using a modified DLVO theory and revealed that the improved performance of carrier flotation was attributed to the enhanced strong aggregation between fine anatase and coarse carrier (i.e., calcite) particles under intense agitation.[8] The advantage of carrier flotation was also reported by Fuerstenau et al.[9] They compared the flotation performance of three flotation techniques on the recovery of ultrafine hematite (<10 μm) from quartz and found that carrier flotation gave the highest recovery and grade of ultrafine hematite particles compared to the other two processes. It was also noted that the preflotation conditioning time in carrier flotation was only two-thirds of that used in the flocculation/flotation process where no carrier particles were present. Moreover, Tabosa et al. reported that considerable improvements, regarding an accelerated kinetics coupled with increases in recovery (17%) and grade (approx. 4%), were achieved in the flotation of copper sulfides when a percentage of the concentrate was recirculated to the rougher flotation feed. The improved separation in this process was

Received: March 13, 2020
Accepted: May 19, 2020
Published: June 2, 2020

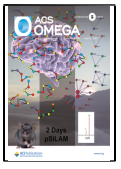

attributed to the increase in collision probability resulting from using hydrophobic copper mineral particles as autogenous carriers in flotation.[10] In addition, compared to conventional flotation, carrier flotation gave higher flotation recovery and lower product ash in the flotation of difficult-to-float/oxidized fine coals, better separation efficiency in separating alunite from kaolin, and higher flotation recovery of fine hematite particles.[11−14]

As discussed in the abovementioned paragraphs, the reviewed literature studies on carrier flotation were of emphases on how to improve flotation recovery and concentration grade. On the other hand, the froth and its stability and the entrainment and the drainage of particles in flotation have been recognized as important factors which affect recovery and grade.[15−17] However, to the best of our knowledge, rare studies have been focused on differentiating the gangue entrainment phenomenon between conventional flotation and carrier flotation. Various kinetic models have been available to optimize and operate the automation of the flotation process.[4,18,19] It is worth to mention that the optimal kinetic flotation model of carrier flotation has never been systematically discussed. In this regard, this study aims to differentiate six different competing models (given in Table 1) employed in carrier flotation and identify the most appropriate model using two different statistical criteria (coefficient of determination, R^2, and root mean square error, RMSE). On the basis, the separation efficiency between conventional and carrier flotation was compared using the optimal kinetic model. Finally, the differences in average sizes of bubbles and water recoveries between conventional and carrier flotation were evaluated.

RESULTS AND DISCUSSION

Optimal Kinetic Model. To find the optimal model for conventional flotation and carrier flotation on the basis of the model fit, kinetic models shown in Table 1 were applied to fit data sets of combustible matter and ash materials obtained from tests. The unknown kinetic parameters (R_∞ and K) were evaluated by the least squares method using nonlinear regression in MATLAB software. This method estimates the values of parameters that minimize the sum of residuals squared across all time points.[21] Meanwhile, two statistical criteria (R^2 and RMSE) were employed to evaluate the model fit. The values of R^2 and RMSE from different models were calculated by programming in MATLAB software.

Figures 1 and 2 plotted the fitting performance (R^2 and RMSE) for conventional flotation and carrier flotation of 51# and 62# coals as a function of flotation kinetic model, respectively. It can be seen that the lowest values of the RMSE and the highest values of R^2 are associated with model 6 (second order with rectangular distribution) irrespective of the reagent scheme, suggesting that model 6 is the best kinetic model from the viewpoint of the model fit, that is, the model is adequate to fit the experimental data in the batch flotation test of 51# and 62# coals.

The experimental data and the predicted results shown in Figures 1 and 2 are represented as time-recovery graphs in Figure 3 to compare the fitting performance among different models. It is obvious that there is little difference among the tested models within one-third of the maximum flotation time (approximately 1 min), which is consistent with the previous research.[25,27,28] However, with a further increase in flotation time, model 6 becomes the most suitable model to describe

Table 1. Description of Applied Flotation Kinetic Models[a]

no.	model	formula	remark
1	classical first-order model	$R = R_{\infty,1}(1 - e^{-K_1 t})$	The classical first-order flotation model is most widely used to optimize the design of flotation circuits. However, the ultimate recovery calculated using this model is smaller than the maximum recovery obtained on the flotation test.[4,19,20]
2	first-order with rectangular distribution	$R = R_{\infty,2}\left[1 - \frac{1 - e^{-K_2 t}}{K_2 t}\right]$	The monodispersed feed with the rectangular distribution of floatabilities was introduced for a better description of the flotation process. In fact, it was proved that this model is a better form of the first-order one.[20−25]
3	fully mixed factor model	$R = R_{\infty,3}\left[1 - \frac{1}{(1 + t/K_3)}\right]$	This model, with the assumption of the exponential distribution of floatabilities, gives an added flexibility over the classical first-order model and enables it to the experimental data very well.[26]
4	improved gas/solid adsorption model	$R = \frac{R_{\infty,4} K_4 t}{1 + K_4 t}$	This model can be derived from the fully mixed reactor model by substituting $1/K_4$ for K_3.
5	second-order model	$R = \frac{R_{\infty,5}^2 K_5 t}{1 + R_{\infty,5} K_5 t}$	The fit-calculated time-recovery profile and the ultimate recovery values are found to be identical to those of fully mixed reactors and the improved gas/solid adsorption model, but this form is not statistically as good as that determined by the first-order forms.[24−27]
6	second-order with rectangular distribution	$R = R_{\infty,6}\left\{1 - \left[\frac{1}{K_6 t}\ln(1 + K_6 t)\right]\right\}$	The fit to the experimental data and the confidence intervals become increasingly worse as the fractional recovery approaches 1.0.[4,25]

[a]Note: subscript 1, 2, 3, 4, 5, and 6 represent model 1, 2, 3, 4, 5, and 6, respectively.

https://dx.doi.org/10.1021/acsomega.0c01116
ACS Omega 2020, 5, 13813−13821

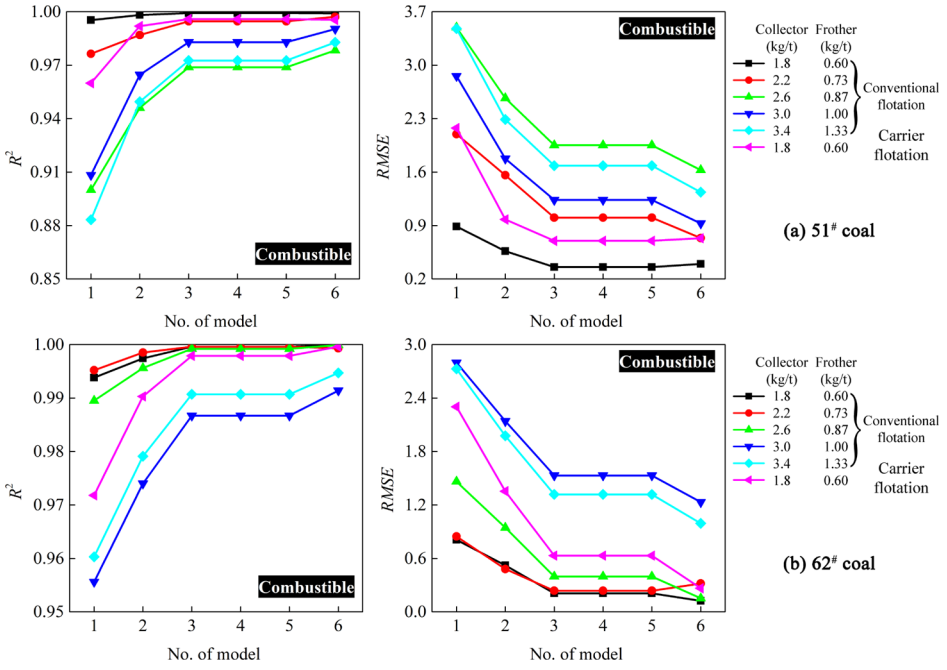

Figure 1. R^2 and RMSE values produced by different kinetic models for combustible recovery of conventional flotation and carrier flotation of (a) 51# and (b) 62# coals.

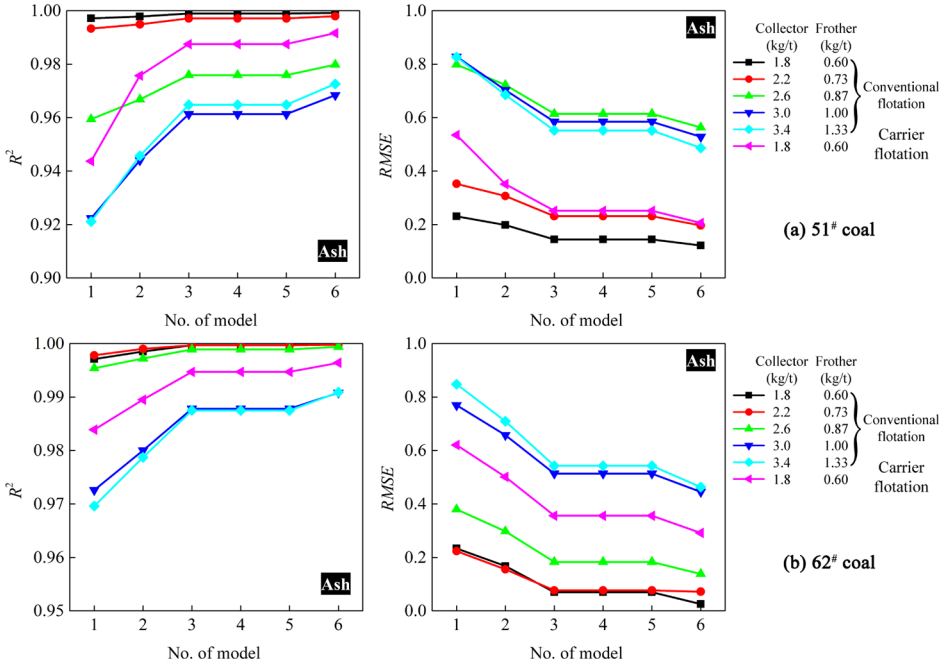

Figure 2. R^2 and RMSE values produced by different kinetic models for ash recovery of conventional flotation and carrier flotation of (a) 51# and (b) 62# coals.

both the processes of conventional flotation and carrier flotation of 51# and 62# coals, that is to say, model 6 is more effective in understanding the overall flotation process than other tested models. Mao et al. reported that model 6 provided the best fit on the experimental data obtained from recovering high-ash lignite by flotation coupled with simultaneous ultrasonic treatment.[29] For the flotation of mixtures including slime particles and coal particles, model 6 was considered as the most reasonable one to fit the flotation results obtained on 0.5−0.25 mm coal particles, among the tested six models.[23] Ni et al. reported that the first-order model with rectangular distribution of floatability was the most reasonable one to fit the rougher and cleaner flotation results attained on a bituminous coal.[24] Bu et al. reported that the representative flotation kinetic models of 375, 188, 100, and 37 μm (average particle sizes) coal particles corresponded to the first order with rectangular distribution, non-integral order, non-integral order, and first order with rectangular distribution, respectively.[4] Thus, the fitting performance of different models may be related to the particle size and also the type of flotation technology.

https://dx.doi.org/10.1021/acsomega.0c01116
ACS Omega 2020, 5, 13813−13821

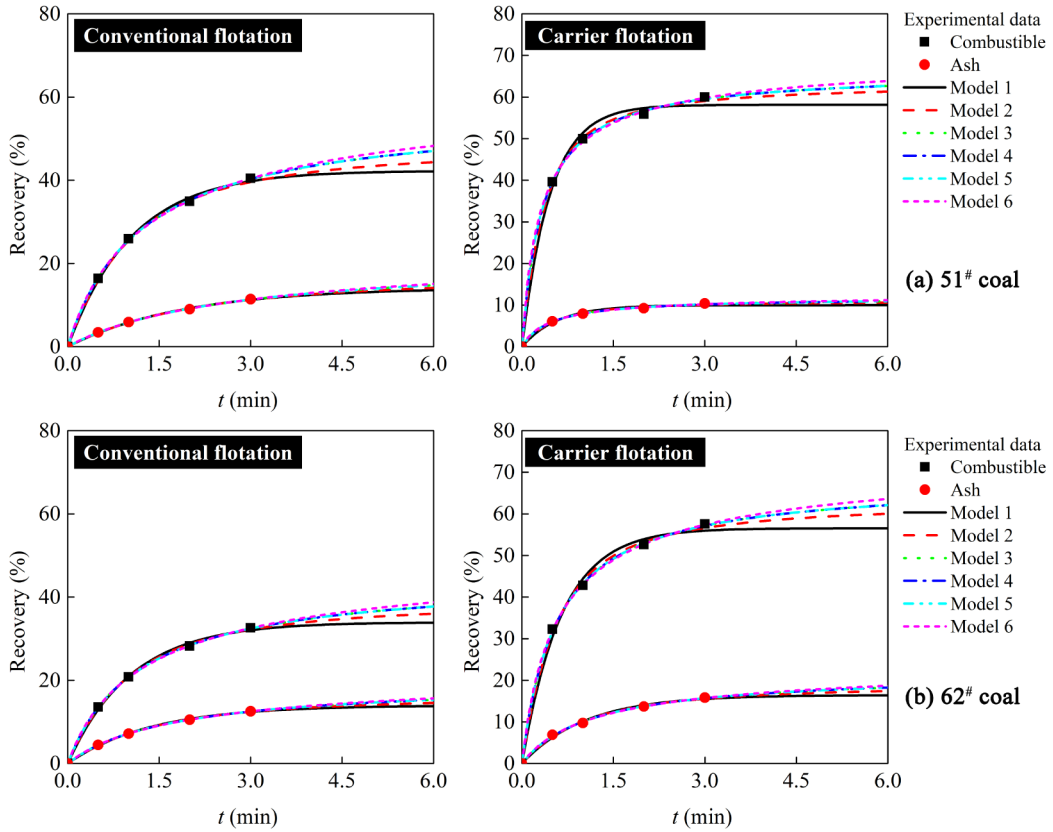

Figure 3. Comparison of different kinetic models fitted to the experimental data of (a) 51# and (b) 62# coals. The fitting curves obtained from models 3, 4, and 5 were overlapped completely.

Table 2. Flotation Kinetic Parameters (R_∞ and K) of Model 6 for 51# Coal

		conventional flotation				carrier flotation			
		combustible		ash		combustible		ash	
collector (kg/t)	frother (kg/t)	R_∞	K	R_∞	K	R_∞	K	R_∞	K
1.80	0.60	64.44	1.548	25.46	0.650	70.18	6.945	12.74	4.475
2.20	0.73	69.08	2.188	23.92	0.850				
2.60	0.87	62.73	4.447	20.61	1.315				
3.00	1.00	59.86	6.439	15.12	2.267				
3.40	1.13	65.13	6.582	15.21	2.597				

The calculated values of R_∞ and K for the six kinetic models are summarized in the Supporting Information. It is noted that the models, including the fully mixed factor model (model 3), the improved gas/solid adsorption model (model 4), and the second-order model (model 5), share the same fitting performance for each time-recovery profile.

Model 3 can be transferred into model 4 by substituting $1/K_3$ for K_4

$$R = R_{\infty,3}\left[1 - \frac{1}{(1 + t/K_3)}\right] = \frac{R_{\infty,3}(1/K_3)t}{1 + (1/K_3)t} = \frac{R_{\infty,4}K_4 t}{1 + K_4 t} \quad (1)$$

$$K_4 = 1/K_3 \quad (2)$$

Meanwhile, model 4 can be derived from model 5 by replacing K_4 with $R_{\infty,5}K_5$.

$$R = \frac{{R_{\infty,5}}^2 K_5 t}{1 + R_{\infty,5}K_5 t} = \frac{R_{\infty,5}(R_{\infty,5}K_5)t}{1 + (R_{\infty,5}K_5)t} = \frac{R_{\infty,4}K_4 t}{1 + K_4 t} \quad (3)$$

$$K_4 = R_{\infty,5}K_5 \quad (4)$$

According to R_∞ and K values of the Supporting Information, the calculated values of $1/K_3$ and $R_{\infty,5}K_5$ were found to be equal to the values of K_4. In addition, the R_∞ values were found to be identical to those of the fully mixed reactors and the improved gas/solid adsorption model. Thus, it was concluded that the equations that can describe model 3, model 4, and model 5 were the same from the viewpoint of mathematics. This explains why the fitting curves for models 3, 4, and 5 are overlapped completely, as observed in Figure 3.

As stated earlier, model 6 was the optimal kinetic model among the six competing models on the basis of the model fit. Therefore, the second-order model with rectangular distribution (model 6) was employed to compare the separation performance between conventional flotation and carrier flotation.

Comparison of Flotation Kinetics between Conventional Flotation and Carrier Flotation. As both the recovery and rate of recovery of combustible matter and ash

https://dx.doi.org/10.1021/acsomega.0c01116
ACS Omega 2020, 5, 13813−13821

Table 3. Flotation Kinetic Parameters (R_∞ and K) of Model 6 for 62# Coal

		conventional flotation				carrier flotation			
		combustible		ash		combustible		ash	
collector (kg/t)	frother (kg/t)	R_∞	K	R_∞	K	R_∞	K	R_∞	K
1.80	0.60	51.34	1.601	23.01	1.030	74.11	3.676	24.72	1.623
2.20	0.73	61.07	1.723	25.42	0.990				
2.60	0.87	71.41	2.048	29.22	1.089				
3.00	1.00	68.65	2.674	23.75	1.493				
3.40	1.13	71.47	2.938	24.68	1.686				

Table 4. Calculated Values of K_m and SI for 51# and 62# Coals

	51# coal			62# coal		
flotation method	$K_{m,com}$	$K_{m,ash}$	SI	$K_{m,com}$	$K_{m,ash}$	SI
conventional	0.9973	0.1655	6.025	0.8221	0.2371	3.468
carrier	4.874	0.570	8.551	2.724	0.401	6.788

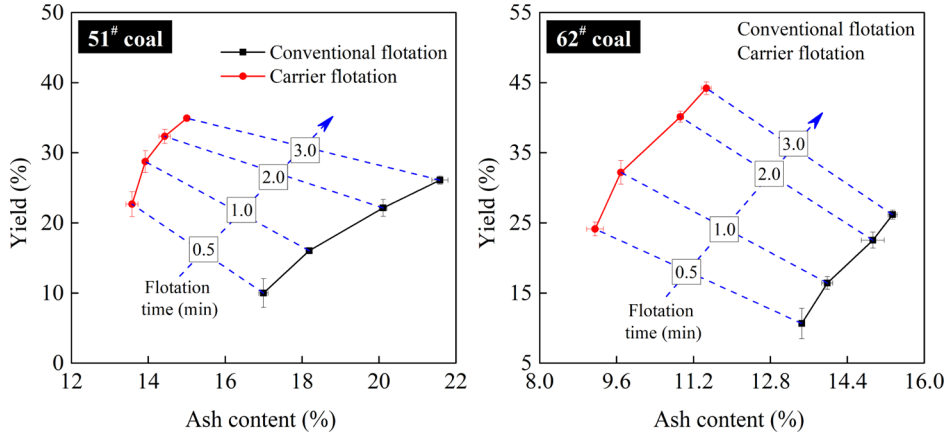

Figure 4. Plots of yields and ash contents of flotation concentrates obtained at various flotation times (1.8 kg/t collector and 0.6 kg/t frother).

materials can be used to evaluate the difference in flotation performance of conventional flotation and carrier flotation, the values of kinetic parameters (R_∞ and K) of model 6 are calculated and shown in Tables 2 and 3. For conventional flotation of 51# and 62# coals, increases in flotation rate constants of combustible matter and ash material were obtained with the increase in collector and frother dosages. The increase in flotation rate constant was attributed to the fact that increasing collector dosage would enhance the collision probability between coal particles and oil droplets because of the enhanced adsorption of the collector on coal surfaces.[30] Thus, more and more coal particles can be reported to the concentrate. Meanwhile, with the increase in combustible recovery, more and more ash materials disseminated with combustible matter were also been recovered, which led to the increase in flotation rate constant of the ash material.

The two kinetic model parameters (R_∞ and K) determined from a recovery-time set of data are effectively used to evaluate the effect of variables on the flotation process. However, it is difficult to compare flotation model parameters among tests or to establish a trend for R_∞ and K values under some conditions.[31−34] The modified flotation rate constant is an approach to compare total flotation response[33]

$$K_m(\mathrm{min}^{-1}) = \frac{R_\infty \times K}{100} \quad (5)$$

On the basis of this modified rate constant, a selectivity index between combustible matter and ash materials is defined as the ratio of their modified rate constants[33]

$$\mathrm{SI(combustible/ash)} = \frac{K_{m,com}}{K_{m,ash}} \quad (6)$$

where $K_{m,com}$, and $K_{m,ash}$ are the modified flotation rate constants of combustible matter and ash materials, respectively.

A change in collector dosage leads to the change in both R_∞ and K values for both combustible matter and ash material. Therefore, the modified flotation rate (K_m) and separation index (SI) were employed to compare the flotation performance between conventional flotation and carrier flotation. The modified flotation rate constant and separation indices were calculated using eqs 1 and 2, according to Tables 2 and 3. Calculated values of K_m and SI for 51# and 62# coals at 1.80 kg/t collector dosage and 0.60 kg/t frother dosage are shown in Table 4. The values of K_m for both combustible matter and ash material obtained from carrier flotation were greater than those of conventional flotation. In addition, it was seen that the increasing degree of $K_{m,com}$ was more significant (from 1.00 to 4.87) than that of $K_{m,ash}$ (from 0.17 to 0.57). This was in agreement with the finding that carrier flotation had a better separation selectivity of −74 μm coal fines over conventional flotation.

https://dx.doi.org/10.1021/acsomega.0c01116
ACS Omega 2020, 5, 13813−13821

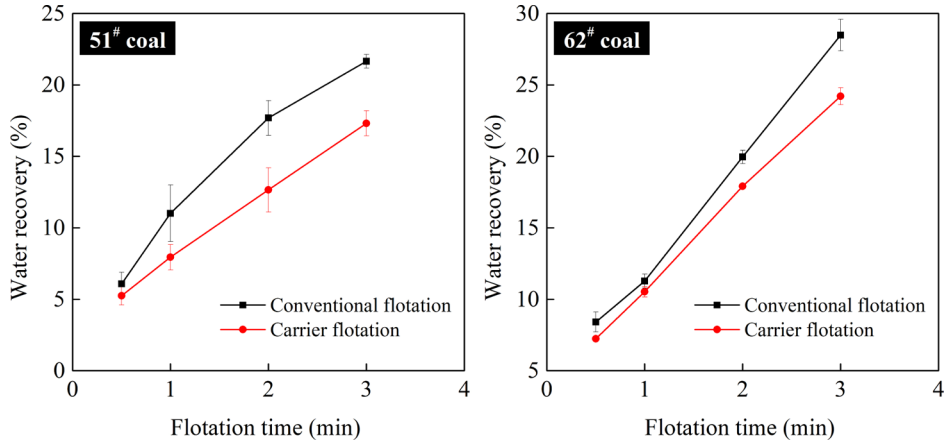

Figure 5. Water recovery as a function of flotation time of conventional flotation and carrier flotation (1.8 kg/t collector and 0.6 kg/t frother).

Figure 4 shows the cumulative yields as a function of cumulative ash contents of flotation concentrates obtained at various flotation time periods. Compared to conventional flotation, the froth concentrate achieved by carrier flotation had a lower ash content and a greater yield at a fixed flotation time. The ash content of 51# coal was reduced from 50.51 to 15.00% at a yield of 34.93% using carrier flotation, while the least ash content of the concentrate obtained from conventional flotation was 17.00% at a yield of 9.99%. For 62# coal, carrier floatation also had superior ability to reduce the ash content and improve the yield of the concentrate compared to conventional flotation. Hence, carrier flotation had higher separation indices for 51# and 62# coals. The better separation selectivity of carrier flotation can be due to the high collision and attachment probabilities between bubbles and the formed aggregate of fine and carrier particles.[7,35] According to Chia and Somasundaran,[8] the selective aggregation of anastase (fine particles) and calcite (carrier particles) can be achieved by a strong chemisorption of the oleate on surfaces of anastase and calcite particles. This phenomenon observed is in good agreement with the calculated results of the extended Derjaguin−Landau−Verwey−Overbeek (EDLVO) theory and the aggregation theory. Similar reports have also been provided by other researchers.[14,36]

Comparison of Froth Properties between Conventional Flotation and Carrier Flotation. In addition, it is worth to note the changes in the water recovery, froth properties, and entrainment of gangue between carrier flotation and conventional flotation.

In general, the recovery of fine particles is primarily due to water recovery or entrainment rather than true flotation via bubble attachment, which can be considered as a dictation of the entrainment of fine particles.[37] As particle size decreases, the water recovery appears to be significantly increased.[38] Figure 5 gives the plots of flotation time versus water recovery of conventional flotation and carrier flotation. It is noted that the presence of 500−250 μm coal particles caused a lower water recovery in carrier flotation as compared to that in conventional flotation of 74 μm fine coal. It is observed in Table 5 that the contact angle of carrier particles is greater than 90°. Crawford and Ralston found that particles with a contact angle larger than 90° were acting as a foam breaking agent.[39] As depicted in Figure 6, the bridging dewetting of the particles due to a large contact angle causes the interface to come into contact and rupture.[40] The strongly hydrophobic carrier

Table 5. Contact Angle Measurement Results of Fine Coals (51# and 62# Coals) and Carrier Particles

	fine particles		
sample	51# coal	62# coal	carrier particles
contact angle (°)	30.53 ± 1.35	33.42 ± 0.96	96 ± 2.24

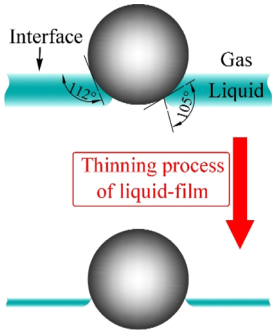

Figure 6. Schematic diagram of a thin liquid film resulting from the dewetting of a hydrophobic particle with a contact angle larger than 90°. Adapted from the literature.[42]

particles can accelerate the drainage of the iner-film, which led to horrible bubble breakup and coalescence. This phenomenon is in agreement with that the average size of bubbles (0.29 ± 0.14 cm) in the top of the froth zone of carrier flotation was larger than that of conventional flotation, as shown in Figure 7. Meanwhile, the drainage of the liquid in the froth can be enhanced by the carrier particles, which is consistent with the difference in water recoveries between conventional flotation and carrier flotation observed in Figure 5. According to Neethling and Cilliers,[41] the coalescence and average size of bubbles have an important effect on the drainage of the liquid in the Plateau borders of the froth. The Plateau borders contain the entrained hydrophilic solids, resulting in the no-selective recovery of gangue materials. The strongly hydrophobic particles presented in carrier flotation are conducive to intensify the drainage of the liquid in the froth and thus decrease the entrainment of gangue materials.

CONCLUSIONS

- All of the six tested flotation kinetic models displayed good fitting performance for experimental results obtained from conventional flotation and carrier

https://dx.doi.org/10.1021/acsomega.0c01116
ACS Omega 2020, 5, 13813−13821

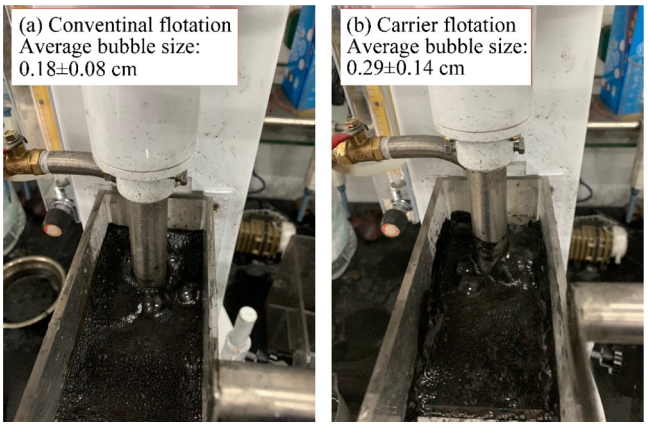

Figure 7. Average sizes of bubbles at the top of the froth zone in the flotation of 51# coal [(a) conventional flotation; (b) carrier flotation]. Images were captured at approximately 5 s after the introduction of air. The average bubble sizes were estimated by manual inspection using ImageJ software.

flotation tests carried out with a short flotation time (<1 min). However, the second-order model (model 6) with rectangular distribution was the optimal function to describe the relationship between the flotation time and recovery as the flotation time was over 1 min.

- Carrier flotation had the superior separation selectivity for −74 μm coal fines compared to conventional flotation. At the same dosages of flotation reagents, the modified flotation rate constants for carrier flotation were increased by three to four times than those of conventional flotation.
- Compared to conventional flotation, carrier flotation using hydrophobic coal particles (contact angle greater than 90°) as carriers led to a larger average size of bubbles because of the acceleration effect of the drainage of the liquid film in the froth. This facilitated the decrease in water recovery and, therefore, the reduction of the gangue entrainment.

EXPERIMENTAL SECTION

Materials. The samples used in this study were coking coals collected from 51# and 62# coal seams of the Shanbula Coal Mine (Ordos, Inner Mongolia, China). The raw coals were subjected to wet screening using a sieve of 74 μm aperture, with the screen underflow being used for conventional and carrier flotation tests. Table 6 gives the proximate analysis results for the three coal samples. The ash contents of the −74 μm size fraction in 51# and 62# coals were 50.51 and 32.97%, respectively. In addition, a narrow size fraction of the 500−250 μm coal sample assaying 6.90% ash content was prepared by screening the dense medium cyclone overflow (clean coal) obtained from the Shanghaimiao Central Coal Preparation Plant (Ordos, Inner Mongolia, China). As shown in previous literature,[43] this narrow-sized coal sample has a good floatability, and thus, it was used as carrier particles in this study.

Table 6. Proximate Analysis for the Three Coal Samples (wt %).[a]

sample	M_{ad}	A_d	V_{daf}	FC_d
51# coal	2.23	50.51	36.73	31.31
62# coal	2.87	32.97	36.21	42.75
carrier	1.67	6.90	40.31	55.57

[a]Note: M_{ad} is moisture content of air-dry basis; A_d is ash content of dry basis; V_{daf} is volatile matter content of dry ash-free basis; FC_d is fixed carbon content of dry basis.

Flotation Tests. A standard laboratory RK/FD-II subaeration flotation cell (volume of 0.5 L) was used for the flotation tests. The air flow rate and impeller speed were maintained at 1.13 cm/s and 1900 rpm, respectively. For all flotation tests, tap water was added to maintain a constant pulp level and froth layer of 1 cm. Kerosene and sec-octyl alcohol were used as the collector and frother, respectively, for all flotation tests. For a typical flotation test, the mass of coal particles was 30 g, which resulted in a solid concentration of 60 g/L. According to the literature,[14] the mass ratio between the carrier particles and the fine coal particles was set at 1:1 for carrier flotation tests. In a given conventional flotation test, the pulp was first agitated in the flotation cell for 1 min. After that, known amounts of collector and frother were added in order, and the slurry was conditioned for 2 and 1 min, respectively. Upon the completion of slurry conditioning, air was introduced and flotation concentrates were collected after cumulative times of 0.5, 1, 2, and 3 min. In carrier flotation tests, in order to determine the recovery for fine coal, coarser carrier particles were separated from the recovered fine coal particles by screening the concentrate products using a sieve of 125 μm aperture. A detailed description of the working process of the mechanical flotation cell has been reported in the literature.[4] Equations 3 and 4 were used to calculate the combustible matter and ash material recoveries in the concentrates.

$$\text{Combustible recovery (\%)} = \frac{\gamma_C(100 - A_C)}{(100 - A_F)} \times 100 \quad (7)$$

$$\text{Ash recovery (\%)} = \frac{\gamma_C A_C}{A_F} \times 100 \quad (8)$$

where the subscript C refers to the concentrate, the subscript F represents the feed, γ_C is the yield of the concentrate, and A is the ash content.

Equation 5 was used to calculate the water recovery in the concentrates.

$$\text{Water recovery (\%)} = \frac{W_C}{W_F} \times 100 \quad (9)$$

where W_C is the weight of water covered in various flotation times and W_F is the total weight of water used in the flotation test.

Contact Angle Measurement. Prior to measuring contact angles, 51# and 62# coals of size intervals of 74−45 μm were obtained via wet screening and were prepared as thin circular plates. The coal plates were obtained by pressing approximately 1 g of the sample in a machine for 50 s under 15 MPa. A JC2000D contact angle analyzer (Powereach, Shanghai, China) was then utilized to measure water contact angles over coal plates by the method of sessile drop. The image of the droplet in contact with the coal sheet at 0.5 s was recorded using the "image analysis method" function given by the software associated with the analyzer, and the value of the contact angle was determined. Each measurement was repeated three times with changing the water drop contacting

https://dx.doi.org/10.1021/acsomega.0c01116
ACS Omega 2020, 5, 13813−13821

positions on the sheet, and the average value of the three tests was taken as the sample's contact angle.

In our previously published article,[43] the collectorless flotation recoveries on the same coal sample (carrier particles) used in this study were constant at approximately 90% regardless of varying particle sizes from 250 to 45 μm. Thus, it is reasonable to assume that there should be no difference in hydrophobicity after subjecting the coarse carrier particles to grinding. The carrier particles (500−250 μm coal particles) were ground to obtain a narrow size fraction of 74−45 μm and then pressed to form coal sheets for contact angle measurements. The measurement result obtained on the 74−45 μm ground product was approximately employed to represent the contact angle of the carrier particles.

■ ASSOCIATED CONTENT

Supporting Information

The Supporting Information is available free of charge at https://pubs.acs.org/doi/10.1021/acsomega.0c01116.

Calculated values of R_∞ and K for the six kinetic models (PDF)

■ AUTHOR INFORMATION

Corresponding Authors

Xiangning Bu − *Key Laboratory of Coal Processing and Efficient Utilization (Ministry of Education), School of Chemical Engineering and Technology, Xuzhou 221116, China;* orcid.org/0000-0001-6291-7656; Email: xiangning.bu@foxmail.com

Biao Li − *Mining and Minerals Engineering Department, Virginia Polytechnic Institute and State University, Blacksburg, Virginia 24060, United States*; Email: biaoli@vt.edu

Authors

Xuexia Wang − *Key Laboratory of Coal Processing and Efficient Utilization (Ministry of Education), School of Chemical Engineering and Technology, Xuzhou 221116, China*

Shaoqi Zhou − *Key Laboratory of Coal Processing and Efficient Utilization (Ministry of Education), School of Chemical Engineering and Technology, Xuzhou 221116, China*

Hanhui Zhan − *School of Environment Science and Spatial Informatics, China University of Mining and Technology, Xuzhou 221116, China*

Guangyuan Xie − *Key Laboratory of Coal Processing and Efficient Utilization (Ministry of Education), School of Chemical Engineering and Technology, Xuzhou 221116, China*

Complete contact information is available at: https://pubs.acs.org/10.1021/acsomega.0c01116

Notes

The authors declare no competing financial interest.

■ ACKNOWLEDGMENTS

The authors gratefully acknowledge financial support from the project funded by the China Postdoctoral Science Foundation (no. 2019M652024).

■ REFERENCES

(1) Zhou, S.; Wang, X.; Bu, X.; Wang, M.; An, B.; Shao, H.; Ni, C.; Peng, Y.; Xie, G. A novel flotation technique combining carrier flotation and cavitation bubbles to enhance separation efficiency of ultra-fine particles. *Ultrason. Sonochem.* **2020**, *64*, 105005.

(2) Trahar, W. J.; Warren, L. J. The flotability of very fine particles - A review. *Int. J. Miner. Process.* **1976**, *3*, 103−131.

(3) Abkhoshk, E.; Kor, M.; Rezai, B. A study on the effect of particle size on coal flotation kinetics using fuzzy logic. *Expert Syst. Appl.* **2010**, *37*, 5201−5207.

(4) Bu, X.; Xie, G.; Chen, Y.; Ni, C. The order of kinetic models in coal fines flotation. *Int. J. Coal Prep. Util.* **2017**, *37*, 113−123.

(5) Miettinen, T.; Ralston, J.; Fornasiero, D. The limits of fine particle flotation. *Miner. Eng.* **2010**, *23*, 420−437.

(6) Greene, E. W.; Duke, J. B. Selective froth flotation of ultrafine minerals or slimes. *Trans. Am. Inst. Min., Metall. Pet. Eng.* **1962**, *223*, 389−395.

(7) Eckert, K.; Schach, E.; Gerbeth, G.; Rudolph, M. Carrier Flotation: State of the Art and its Potential for the Separation of Fine and Ultrafine Mineral Particles. *Mater. Sci. Forum* **2019**, *959*, 125−133.

(8) Chia, Y. H.; Somasundaran, P. A theoretical approach to flocculation in carrier flotation for beneficiation of clay. *Colloids Surf.* **1983**, *8*, 187−202.

(9) Fuerstenau, D. W.; Li, C.; Hanson, J. S. Shear flocculation and carrier flotation of fine hematite. In *Production and Processing of Fine Particles*; Elsevier: Amsterdam, 1988; pp 329−335.

(10) Tabosa, E.; Rubio, J. Flotation of copper sulphides assisted by high intensity conditioning (HIC) and concentrate recirculation. *Miner. Eng.* **2010**, *23*, 1198−1206.

(11) Ateşok, G.; Boylu, F.; Çelik, M. Carrier flotation for desulfurization and deashing of difficult-to-float coals. *Miner. Eng.* **2001**, *14*, 661−670.

(12) Yang, H.; Cai, Y.; Wu, L. Flotation behavior of raw and oxidized fine coal when mixed with coarse particles. *Fuel* **2018**, *232*, 225−232.

(13) Koca, S.; Koca, H. Carrier flotation of alunite from kaolin clay. *Dev. Miner. Process.* **2000**, *13*, C11.

(14) Li, D.; Yin, W.; Liu, Q.; Cao, S.; Sun, Q.; Zhao, C.; Yao, J. Interactions between fine and coarse hematite particles in aqueous suspension and their implications for flotation. *Miner. Eng.* **2017**, *114*, 74−81.

(15) Bu, X.; Zhang, T.; Chen, Y.; Peng, Y.; Xie, G.; Wu, E. Comparison of mechanical flotation cell and cyclonic microbubble flotation column in terms of separation performance for fine graphite. *Physicochem. Probl. Miner. Process.* **2018**, *54*, 732−740.

(16) Wang, L.; Peng, Y.; Runge, K.; Bradshaw, D. A review of entrainment: Mechanisms, contributing factors and modelling in flotation. *Miner. Eng.* **2015**, *70*, 77−91.

(17) Bu, X.; Zhang, T.; Peng, Y.; Xie, G.; Wu, E. Multi-stage flotation for the removal of ash from fine graphite using mechanical and centrifugal forces. *Minerals* **2018**, *8*, 15.

(18) Luttrell, G. H.; Yoon, R. H. Automation of a laboratory flotation machine for improved performance. *Int. J. Miner. Process.* **1983**, *10*, 165−172.

(19) Bu, X.; Xie, G.; Peng, Y.; Ge, L.; Ni, C. Kinetics of flotation. Order of process, rate constant distribution and ultimate recovery. *Physicochem. Probl. Miner. Process.* **2017**, *53*, 342−365.

(20) Mazumdar, M. Statistical discrimination of flotation models based on batch flotation data. *Int. J. Miner. Process.* **1994**, *42*, 53−73.

(21) Ahmed, M. M. Discrimination of different models in the flotation of Maghara coal. *Miner. Process. Extr. Metall.* **2004**, *113*, 103−110.

(22) Bayat, O.; Ucurum, M.; Poole, C. Effects of size distribution on flotation kinetics of Turkish sphalerite. *Miner. Process. Extr. Metall.* **2004**, *113*, 53−59.

(23) Ni, C.; Bu, X.; Xia, W.; Peng, Y.; Xie, G. Effect of slimes on the flotation recovery and kinetics of coal particles. *Fuel* **2018**, *220*, 159−166.

(24) Ni, C.; Xie, G.; Jin, M.; Peng, Y.; Xia, W. The difference in flotation kinetics of various size fractions of bituminous coal between rougher and cleaner flotation processes. *Powder Technol.* **2016**, *292*, 210−216.

(25) Yuan, X.-M.; Palsson, B. I.; Forssberg, K. S. E. Statistical interpretation of flotation kinetics for a complex sulphide ore. *Miner. Eng.* **1996**, *9*, 429−442.
(26) Dowling, E. C.; Klimpel, R. R.; Aplan, F. F. Model discrimination in the flotation of a porphyry copper ore. *Trans. Soc. Min., Metall., Explor.* **1985**, *2*, 87−101.
(27) Bu, X.; Xie, G.; Peng, Y.; Chen, Y. Kinetic modeling and optimization of flotation process in a cyclonic microbubble flotation column using composite central design methodology. *Int. J. Miner. Process.* **2016**, *157*, 175−183.
(28) Stanojlović, R. D.; Sokolović, J. M. A study of the optimal model of the flotation kinetics of copper slag from copper mine Bor. *Arch. Min. Sci.* **2014**, *59*, 821−834.
(29) Mao, Y.; Bu, X.; Peng, Y.; Tian, F.; Xie, G. Effects of simultaneous ultrasonic treatment on the separation selectivity and flotation kinetics of high-ash lignite. *Fuel* **2020**, *259*, 116270.
(30) Chaudhuri, S.; Kalyani, V. K.; Charan, T. G.; Kumari, S.; Sinha, A. Improved collector for beneficiation of low-volatile medium ash clean coal fines by froth flotation. *Int. J. Coal Prep. Util.* **2014**, *34*, 321−331.
(31) Marion, C.; Jordens, A.; Li, R.; Rudolph, M.; Waters, K. E. An evaluation of hydroxamate collectors for malachite flotation. *Sep. Purif. Technol.* **2017**, *183*, 258−269.
(32) Oney, O.; Samanli, S.; Celik, H.; Tayyar, N. Optimization of operating parameters for flotation of fine coal using box-behnken design. *Int. J. Coal Prep. Util.* **2015**, *35*, 233−246.
(33) Xu, M. Modified flotation rate constant and selectivity index. *Miner. Eng.* **1998**, *11*, 271−278.
(34) Yin, Z.; Xu, L.; He, J.; Wu, H.; Fang, S.; Khoso, S. A.; Hu, Y.; Sun, W. Evaluation of l-cysteine as an eco-friendly depressant for the selective separation of MoS2 from PbS by flotation. *J. Mol. Liq.* **2019**, *282*, 177−186.
(35) Rubio, J.; Hoberg, H. The process of separation of fine mineral particles by flotation with hydrophobic polymeric carrier. *Int. J. Miner. Process.* **1993**, *37*, 109−122.
(36) Yao, J.; Xue, J.; Li, D.; Fu, Y.; Gong, E.; Yin, W. Effects of fine−coarse particles interaction on flotation separation and interaction energy calculation. *Part. Sci. Technol.* **2018**, *36*, 11−19.
(37) Feng, D.; Aldrich, C. Effect of particle size on flotation performance of complex sulphide ores. *Miner. Eng.* **1999**, *12*, 721−731.
(38) Bu, X.; Xie, G.; Peng, Y. Interaction of fine, medium, and coarse particles in coal fines flotation. *Energy Sources, Part A* **2017**, *39*, 1276−1282.
(39) Crawford, R.; Ralston, J. The influence of particle size and contact angle in mineral flotation. *Int. J. Miner. Process.* **1988**, *23*, 1−24.
(40) Hunter, T. N.; Pugh, R. J.; Franks, G. V.; Jameson, G. J. The role of particles in stabilising foams and emulsions. *Adv. Colloid Interface Sci.* **2008**, *137*, 57−81.
(41) Neethling, S. J.; Cilliers, J. J. The entrainment of gangue into a flotation froth. *Int. J. Miner. Process.* **2002**, *64*, 123−134.
(42) Aveyard, R.; Binks, B. P.; Fletcher, P. D. I.; Peck, T. G.; Rutherford, C. E. Aspects of aqueous foam stability in the presence of hydrocarbon oils and solid particles. *Adv. Colloid Interface Sci.* **1994**, *48*, 93−120.
(43) Bu, X.; Chen, Y.; Ma, G.; Sun, Y.; Ni, C.; Xie, G. Differences in dry and wet grinding with a high solid concentration of coking coal using a laboratory conical ball mill: Breakage rate, morphological characterization, and induction time. *Adv. Powder Technol.* **2019**, *30*, 2703−2711.

https://dx.doi.org/10.1021/acsomega.0c01116
ACS Omega 2020, 5, 13813−13821